Sustainable Food Proteins

WILEY

AOCS
Your Global Fats and Oils Connection

ORIGINAL ARTICLE OPEN ACCESS

Quinoa Protein Concentrate as a Platform for the Protection and Controlled Delivery of Resveratrol and Tocopherol

Alejandra J. Rubinstein[1] | Guadalupe Garcia Liñares[2] | Valeria Boeris[3] | Oscar E. Pérez[1]

[1]Departamento de Química Biológica, Facultad de Ciencias Exactas y Naturales, Consejo Nacional de Investigación Científica y Técnicas de la República Argentina, IQUIBICEN-CONICET. Universidad de Buenos Aires, Buenos Aires, Argentina | [2]Laboratorio de Biocatálisis, Departamento de Química Orgánica y UMYMFOR, Facultad de Ciencias Exactas y Naturales, Universidad de Buenos Aires-CONICET, Buenos Aires, Argentina | [3]Área Fisicoquímica, Departamento de Química Física, Facultad de Ciencias Bioquímicas y Farmacéuticas, Universidad Nacional de Rosario (UNR)–CONICET, Rosario, Argentina

Correspondence: Oscar E. Pérez (oscarperez@qb.fcen.uba.ar)

Received: 12 September 2025 | **Revised:** 25 March 2026 | **Accepted:** 8 April 2026

Keywords: complexation | quinoa proteins | resveratrol | tocopherol

ABSTRACT

The objective of this work was to generate and characterize complexes of quinoa proteins (QP) with either resveratrol (RSV) or tocopherol (TOC) whose dimensions fell into the nanoscale. The QP-based nanocomplexes characterization was carried out jointly with encapsulation efficiency determination. Fourier-Transform Infrared Spectroscopy (FTIR) showed no covalent bond formation and indicated that the protein's secondary structure was modified. Transmission Electron Microscopy (TEM) images and Dynamic Light Scattering (DLS) measurements confirmed that the addition of bioactive compounds did not substantially alter the protein's original size. A consistent particle diameter of 100 nm was observed in both types of nanocomplexes with and without RSV and TOC. The antioxidant capacity of nanocomplexes was analyzed after an in vitro simulated digestion process, showing an increase in this property postdigestion. These nanocomplexes hold great potential as functional ingredients.

1 | Introduction

Quinoa (*Chenopodium quinoa Willd.*) is a traditional pseudocereal species, native to the Andean highlands of South America. In recent years, quinoa seeds have garnered significant attention due to their outstanding nutritional profile, particularly their high-quality protein content and abundance of antioxidant compounds (He et al. 2022; Lingiardi et al. 2022). While, resveratrol (RSV), or 3,5,4′-trihydroxystilbene, is a nonflavonoid polyphenol that naturally exists in both *trans* and *cis* isomeric forms. It is predominantly found in the skins of grapes, blueberries, mulberries, and various other plant sources (Buosi et al. 2020). Despite its recognized physiological benefits, RSV exhibits poor physicochemical stability and unfavorable pharmacokinetic properties. Its high sensitivity to oxidative environments results in rapid degradation and extensive metabolism, ultimately limiting its bioavailability. These limitations underscore the critical need for advanced delivery systems capable of preserving the bioactivity of RSV and enhancing its functional efficacy (Chimento et al. 2019). Conversely, α-tocopherol (TOC) is the most active and biologically relevant form of lipophilic vitamin E, widely studied for its role in reducing the risk of chronic diseases associated with oxidative stress (Shahidi and De Camargo 2016). However, its application is hindered by its hydrophobic nature and susceptibility to degradation by oxygen, heat, and light (Saini and Keum 2016).

Proteins possess the intrinsic ability to self-assemble into supramolecular structures under specific environmental conditions such as pH, ionic strength, temperature, concentration, or upon interaction with small ligands (Martínez et al. 2019). When a bioactive molecule, such as a vitamin (ligand), binds to a protein, a new complex may form, which can further aggregate through self-assembly processes. This leads to the development

of nanostructures known as nanocomplexes—versatile delivery systems capable of encapsulating and transporting a wide range of bioactive compounds. A particularly promising feature of these nanocomplexes is their ability to encapsulate and release preloaded compounds such as RSV or TOC in targeted environments.

In previous studies, it was demonstrated that QP formed complexes with RSV and TOC, and furthermore, that the interaction between QP-RSV is stronger than QP-TOC (Rubinstein and Pérez 2025). Also, the 11S quinoa protein (QP) was purified, and its complexation with RSV and TOC was studied (Rubinstein et al. 2024). In this context, this study aimed to design and characterize nanocomplexes based on QP as a platform for RSV or TOC encapsulation, controlled delivery and protection, evaluated in terms of their antioxidant capacity conservation upon simulated gastrointestinal digestion.

2 | Materials and Methods

2.1 | Materials

Defatted Peruvian quinoa (*C. quinoa* Willd.) seed flour was sourced from "El Portugués" (Buenos Aires, Argentina). QP concentrate was extracted from the defatted flour following the protocol described by Martínez et al. (2019). The composition of the quinoa concentrate was determined to be 10% protein, 3% fat, 1% fiber, and 1% carbohydrates on a wet basis (Rubinstein and Pérez 2025). The electrophoretic profile of the QP isolate was previously analyzed in an earlier study (Rubinstein et al. 2024). α-TOC was kindly provided by DSM Laboratories, and RSV was generously supplied by Temis Lostaló, both companies located in Argentina. Both bioactive compounds were used without further purification. Milli-Q grade water was used throughout all procedures. All reagents were of analytical grade.

2.2 | Preparation of Solutions: QP, TOC, RSV, and Their Mixtures

Solutions of QP and either RSV or TOC were prepared separately by dissolving each compound in its respective solvent, followed by dilution in distilled water at pH 9 under gentle agitation at room temperature. For the TOC stock solution, 1 g of TOC was weighed and diluted in 10 mL of 96% ethanol. This solution was then diluted with double-distilled water to a final concentration of 30 mM. For the RSV stock solution, 0.00456 g of RSV was dissolved in 1600 μL of 96% ethanol, followed by dilution with double-distilled water to a final volume of 4 mL, yielding a 5 mM solution.

All solutions were freshly prepared and centrifuged at 9100*g* for 10 min at 20°C. The supernatants were stored at 4°C for 24 h to ensure complete hydration of the components. Each mixed system consisting of protein and bioactive (RSV or TOC), forming the nanocarriers, was measured at least twice and elaborated freshly for each measurement instance. QP was consistently prepared from the same quinoa flour batch following a standardized protocol. A stock solution was established, and as it reached depletion, subsequent batches were prepared. In the mixed systems, the final protein concentration was maintained at 1% (w/w), while RSV and TOC concentrations ranged from 100 to 1500 μM. Single QP, TOC or RSV solutions were used as controls.

2.3 | Encapsulation Efficiency (EE)

The amount of RSV or TOC bound to QP was determined by calculating the difference between the initial concentration of the bioactive compound introduced into the system (BIO_N) and the concentration of the unbound (free) compound remaining in the supernatant (BIO_S), according to Rubinstein et al. (2024). The BIO_S value corresponds to the concentration of RSV or TOC present in the supernatant after ultrafiltration using a 10 kDa molecular weight cut-off unit (Vivaspin Turbo 15, Sartorius, Gloucestershire, UK) following centrifugation. For this procedure, 5 mL of each sample (QP-RSV or QP-TOC at 0.5% in distilled water, pH 9) was subjected to centrifugation using ultrafiltration units. A solution containing only the bioactive compound was used as a control to evaluate potential losses due to adsorption to the filter membrane. Ultrafiltration was performed at 4500*g* for 15 min at 24°C using a RC-5 Superspeed refrigerated centrifuge (Sorval, Minneapolis, MN, USA). The filtrate was collected, and the concentration of RSV or TOC was subsequently determined.

RSV concentration was measured via UV–Vis spectrophotometry at 306 nm using a Jasco V-570 instrument (Tokyo, Japan) at 25°C ± 1°C. TOC quantification was performed following the method described Demirkaya and Kadioglu (2007), using an Agilent 7820A gas chromatograph equipped with a flame ionization detector (FID) and G4513A autosampler.

EE (%) for RSV and TOC in the QP-based complexes was then calculated as follows:

$$EE(\%) = \frac{BIO_N - BIO_s}{BIO_N} \times 100 \quad (1)$$

2.4 | Fourier Transform Infrared Spectroscopy (FTIR)

For these assays, a lyophilized powder was used, which was prepared from solutions of 1% QP and 250 μM RSV or 1% QP and 2500 μM TOC. Infrared spectra of lyophilized samples were recorded using a Nicolet IS50 FTIR-ATR spectrometer (Madison, WI, USA) with a range of 4000–400 cm^{-1} and a resolution of 4 cm^{-1}, from solid samples. The data were processed by averaging 32 scans with a resolution of 4 cm^{-1}, using PerkinElmer Spectrum 100 software (Thermo Scientific, Waltham, MA, USA).

2.5 | Circular Dichroism (CD)

For these experiments, QP, and the QP-RSV or QP-TOC mixed solutions were diluted to obtain a final protein concentration of 0.02% (w/w), 10 μM of RSV and 250 μM of TOC, respectively. CD spectra were recorded using a JASCO J-815 CD spectrometer

(Silver Spring, MD, USA) over a wavelength range of 190–260 nm, with a bandwidth of 1 nm. Spectra of the individual bioactive compounds, RSV and TOC, were also acquired; however, no significant CD signals were observed. The percentage of protein secondary structure was estimated using the BestSel deconvolution algorithm (https://bestsel.elte.hu/index.php).

2.6 | Transmission Electron Microscope (TEM)

Samples were analyzed using TEM as described by Buosi et al. (2020). Briefly, 10 μL of the sample was diluted in ultrapure water (1:100 v/v). A 10 μL aliquot of the diluted sample was then mixed with 10 μL of 2% (w/v) uranyl acetate for 3 min. Next, 10 μL of the mixture was placed onto a copper grid and covered with a Formvar film (200 mesh) for 30 s. Excess liquid was removed using filter paper, and the grids were dried in a desiccator. TEM imaging was conducted using a Zeiss 109 instrument with a Gatan ES1000W camera (Carl Zeiss NTS GmbH, Oberkochen, Germany).

2.7 | Particle Size and ζ-Potential Determinations

Dynamic light scattering (DLS) measurements were performed using a Horiba Scientific nanoPartica SZ-100 instrument (Kyoto, Japan), at 25°C. Samples were placed in Hellma quartz glass cuvettes (Müllheim, Germany). Analysis of the intensity fluctuations of the scattered light enabled the calculation of particle diffusion coefficients, from which hydrodynamic diameters were determined via the Stokes–Einstein equation. Data interpretation followed the methodology described by Pérez et al. (2014). For the DLS experiments, RSV concentrations in mixed systems ranged from 5 to 50 μM, meanwhile TOC ranged from 125 to 375 μM.

ζ–Potential measurements were also carried out using the same instrument, with samples loaded into semi-disposable carbon electrode cells (DTS1070, Malvern Panalytical). Electrophoretic mobility values were obtained and converted to ζ–potential using Henry's equation (Rubinstein et al. 2024).

2.8 | In Vitro Digestion Assays

Solutions of single RSV, TOC, QP, and mixed systems, along with their respective controls, were submitted to a simulated gastrointestinal digestion process following the experimental protocol outlined by De Matteo et al. (2024).

Samples of 5 g from each system were taken, and the in vitro digestion assay was performed in duplicate. First, 5 mL of Simulated Salivary Fluid (SSF), composed of various salts at appropriate concentrations to mimic physiological conditions, was added. In this initial oral phase, the ratio between the resuspension and the added solutions (SSF and α-amylase enzyme) was 1:1 (w/v). The pH was adjusted to 7, and the mixture was incubated for 2 min at 37°C.

The process continued with the gastric phase by adding Simulated Gastric Fluid (SGF). Pepsin was incorporated to act on proteins. These solutions were added in a 1:1 ratio relative to the oral phase content, and the sample was adjusted to pH 3. Incubation was carried out for 2 h at 37°C.

The final stage was the intestinal phase. Simulated Intestinal Fluid (SIF) was added, along with bile salts and pancreatin. These solutions were added in a 1:1 ratio relative to the previous gastric content; the pH was adjusted to 7, and the mixture was incubated for 2 h at 37°C. Upon completion, the samples were cooled on ice to inhibit enzymatic activity and subsequently centrifuged to separate the digested extract from the precipitate.

After digestion, samples were centrifuged for 10 min at 4500g, and the resulting supernatants were collected and analyzed for the following test.

2.9 | Antioxidant Activity

2.9.1 | 2,2-Azinobis-(3-Ethylbenzothiazoline-6-Sulfonic Acid) Assay (ABTS)

The antioxidant capacities of the nanocomplexes were assessed through the ABTS assay, as outlined in Rubinstein and Pérez (2025). In this method, the preformed radical monocation of 2,2-azinobis-(3-ethylbenzothiazoline-6-sulfonic acid) (ABTS•+), obtained by oxidizing ABTS with potassium persulfate, serves as a marker. To initiate the process, ABTS was dissolved in water to achieve a final concentration of 7 mM. The ABTS•+ radical cation was generated by reacting to the ABTS stock solution with a final concentration of potassium persulfate of 2.45 mM. The mixture was allowed to stand in darkness at room temperature for 12–16 h before use. The assessment of antioxidant activity for the nanocomplexes was conducted after diluting the ABTS•+ solution with phosphate buffer to achieve an absorbance of 0.80–0.90 (A_0) at 734 nm (V-570, UV–visible Jasco spectrophotometer, Tokyo, Japan). Next, 2.5 mL of this solution was mixed with 0.5 mL of the sample to finally measure the absorbance decrease (A_{inf}). Therefore, ABTS•+ scavenging capacity was calculated as:

$$\text{ABTS scavenging capacity}\,(\%) = \left(\frac{A_0 - A_{inf}}{A_0}\right) * 100 \quad (2)$$

2.9.2 | Ferric Reducing Antioxidant Power (FRAP) Assay

FRAP assay was conducted according to the protocol described by Rubinstein et al. (2024). Aliquots of 40 μL from QP and nanocomplex samples, as well as from a gallic acid (GA) standard solution, were added to test tubes containing 600 μL of freshly prepared FRAP reagent. The reaction mixtures were incubated in the dark at 25°C for 30 min. Subsequently, absorbance was measured at 593 nm using a UV–Vis spectrophotometer (Jasco V-570, Tokyo, Japan).

2.9.3 | Hydrogen Peroxide Scavenging Assay (H_2O_2)

The ability of the samples to scavenge hydrogen peroxide was determined according to the method described by Pleh et al. (2021). Briefly, a 40 mM solution of hydrogen peroxide was

prepared in phosphate buffer (pH 7.4). Various concentrations of samples were added to 0.6 mL of H_2O_2 in solution. The absorbance was measured at 230 nm after 10 min, against a blank solution containing the phosphate buffer without hydrogen peroxide and the percentage inhibition was calculated according to Equation (3), where A_i is the absorbance of the sample, and A_0 the absorbance of the control.

$$\text{Scavenging activity}\,(\%) = \left(1 - \frac{A_i}{A_0}\right) \times 100 \quad (3)$$

2.10 | Statistical Analysis

All experiments were performed at least in triplicate. Results were expressed as mean ± SD. The model's goodness-of-fit was evaluated by the coefficient of determination (R2) using GraphPad Prism 8.0. software.

3 | Results and Discussion

3.1 | EE

In order to measure EE, it is first necessary to ensure that the bioactive compound has been encapsulated. To this end, previous studies have determined that QP formed complexes with TOC and RSV using various techniques such as isothermal titration calorimetry and fluorescence spectroscopy (Rubinstein and Pérez 2025). Therefore, in the current work, it was determined that the EE achieved was 35% for RSV and 19% for TOC. These values are in the same range as those reported by Martínez et al. (2019), who obtained 23% efficiency for the encapsulation of betanin, a pigment known for its potent antioxidant properties, using quinoa 11S globulin.

Although the EE differs from that reported by Rubinstein et al. (2024) for TOC-11S quinoa (19 vs. 73%). It is important to note that there are different affinities between the pairs formed between the encapsulating material and the bioactive compound, given their different chemical natures, such as betanin and TOC. The interactions between them vary, resulting in different encapsulation efficiencies. Here, the QP concentrate contains other constituents, such as carbohydrates and nontarget proteins, which evidently enhance the encapsulation of bioactive compounds. This represents a promising result, as the industrial scaling of purified 11S is cost-prohibitive and practically unfeasible. In contrast, the industrial scale-up of a protein concentrate is more cost-effective and commercially viable.

3.2 | Impact of Complexation on Protein Structure

3.2.1 | FTIR and CD

Fourier-transform infrared spectroscopy (FTIR) is a technique that utilizes infrared radiation to analyze molecular interactions. In this study, FTIR was performed on the pure bioactive compounds, QP, and the QP + RSV and QP + TOC nanocomplexes. Figure S1 shows the spectra obtained for the samples considered. The pure compounds displayed their characteristic spectra, which are consistent with previously reported literature (Akhtar et al. 2022; Roxana Bancuta et al. 2018). In the case of QP, characteristic protein peaks can be observed, such as the amide bond vibration around the 1600 cm^{-1} region. Regarding the complexes, their spectra are very similar to that of QP, indicating that the bioactive compounds were successfully encapsulated. Furthermore, no new peaks were detected, suggesting that the interactions between QP and the bioactive compounds occurred through noncovalent bonding. The most significant modifications in the protein's FTIR spectrum were centered on two main bands that are sensitive to its secondary structure: the Amide I and Amide II bands. The Amide I band, located approximately between 1600 and 1700 cm^{-1}, originates mainly from the carbonyl (C=O) stretching vibrations of the peptide backbone. Changes in this band indicated alterations in secondary structure, including α-helices, β-sheets, turns, and random coils. The Amide II band, located near 1550 cm^{-1}, arises from N-H bending and C-N stretching vibrations and is also sensitive to the protein's conformation (Haris and Chapman 1995).

To elucidate the changes in the protein secondary structure, the second derivative was analyzed and the spectra were deconvoluted in the Amide I region (Figure S2A–C). Based on this analysis, the percentage of protein secondary structure for all three cases were calculated (Bustos et al. 2024). As shown in Figure S2D, the β-sheet structure was predominant in all three samples. Notably, the percentage of β-sheet decreased with the addition of bioactive compounds. Regarding the α-helix, which represents the most ordered structure, it was practically absent in the free protein and with the addition of RSV. However, its presence emerged with the addition of TOC, suggesting that this bioactive contributed to the ordering of the protein structure. Interestingly, each bioactive modified the secondary structure differently, indicating distinct chemical interactions.

Previous reports on quinoa 11S (the major QP) revealed by DC the following secondary structure composition: 0.8% α-helix, 46% β-sheet, 15.9% β-turn, and 36.3% other disordered patterns (Rubinstein et al. 2024). The addition of RSV or TOC in those studies led to a decrease in α-helix, β-sheet, and β-turn content. In that context, the addition of TOC was also recognized to induce system ordering, which was consistent with our previous observations for the concentrated protein. Although the obtained values differ from those reported by Rubinstein et al. (2024), the same trend regarding protein secondary structures is observed: a predominance of β sheets and a near-absence of α-helices. These discrepancies arise because Rubinstein et al. (2024) utilized purified 11S globulin, whereas the present study employs a protein concentrate containing additional constituents alongside the 11S fraction.

The secondary structure of the QP concentrate and the QP-TOC and QP-RSV nanocomplexes was also analyzed by CD. The results are shown in Table 1. As can be seen, the percentages are not exactly the same, as each technique uses different fundamentals to evaluate the secondary structure. Also, FTIR is measured on lyophilized samples, while CD uses samples in solution. Owing to their distinct characteristics, FTIR spectroscopy is better suited for the robust estimation of antiparallel β-sheets,

TABLE 1 | Comparison of secondary structure by FTIR and DC.

	%α HELIX		%β SHEET		%TURN		%OTHERS	
	FTIR	DC	FTIR	DC	FTIR	DC	FTIR	DC
QP	0	0	58.7	41.6	23.3	14.2	18.0	44.2
QP + RSV	0	0	41.7	42.2	18.1	15.1	40.2	42.7
QP + TOC	18.3	0	52.8	40	21.9	13.9	7.0	46.1

whereas CD spectroscopy offers more definitive predictions of α-helix structures (Schwaighofer et al. 2016). However, the general results had the same trend: TOC tends to order the protein structural level, or in this case, it almost did not induce modifications, while RSV slightly increased the percentages of β-sheets and β-turn.

3.2.2 | DLS

To complement these findings, samples were analyzed by DLS to determine the particle size and ζ-potentials of QP, QP-RSV, and QP-TOC nanocomplexes. The particle size results, presented in Table 2, indicate that the increase of RSV or TOC concentrations did not cause significant changes in the hydrodynamic diameter, at least in the studied concentration range of the bioactive compounds.

On the other hand, the protein's zeta potential was measured at −33.70 mV. As shown in Table 2, this value remained practically unchanged upon the addition of either RSV or TOC. Regarding this, the existing literature suggests that electrostatically stabilized hydrocolloids typically possess ζ-potentials surpassing absolute values of 40 mV, as observed by Andreeva et al. (2017). The physical stability of the nanocomplexes is not adequately explained by electrostatic stabilization alone. This implies that their stability is controlled by different forces, which may include hydrophobic, van der Waals, or steric interactions. All the examined systems remained colloidally stable, even those with ζ-potential values less than 40 mV.

TABLE 2 | Mean hydrodynamic diameter and ζ-potentials of QP and mixed systems.

	Z average (nm)	ζ-Potencial (mV)
System	Mean ± SD	Mean ± SD
QP	97 ± 15	−33.70 ± 0.36
QP + RSV 5 μM	80 ± 25	−33.27 ± 0.69
QP + RSV 12.5 μM	100 ± 18	−31.33 ± 1.10
QP + RSV 25 μM	89 ± 20	−30.17 ± 0.60
QP + RSV 37.5 μM	92 ± 18	−35.63 ± 1.10
QP + RSV 50 μM	92 ± 21	−29.80 ± 1.61
QP + TOC 125 μM	103 ± 26	−33.23 ± 2.62
QP + TOC 250 μM	108 ± 11	−30.70 ± 1.51
QP + TOC 375 μM	122 ± 27	−32.23 ± 2.90

3.3 | Microstructure- TEM

TEM is a technique that uses a fine beam of high-speed accelerated electrons as the illumination source, enabling the acquisition of high-resolution images. TEM images were obtained for QP, QP + RSV, and QP + TOC, and they are shown in Figure 1. Additionally, images of single QP, RSV, and TOC were acquired to verify the absence of aggregate formation in these samples (data not shown).

For QP, the image shown in Figure 1A was obtained, including a large number of protein structures with an average diameter of approximately 40 nm. The single protein formed discrete, relatively uniform globular nanoparticles.

The addition of RSV or TOC did not induce significant changes in the QP based nanocomplexes size, as evidenced by the similar results observed in Figure 1B,C compared to the single protein. The observed changes, if any, were too subtle to be detected by this method. This was a significant finding, suggesting that while ligand binding influenced the protein's secondary structure, it does not alter its quaternary structure, that is, QP aggregation. This fact was consistent with what was observed by DLS.

Supporting this finding, Skvarnavičius et al. (2021) demonstrated that upon ligand binding, carbonic anhydrase isozymes I and II exhibited a negative binding volume, which indicates a decrease in the total volume of the protein-ligand complex relative to the unbound state. Considering another type of colloidal system, the impact of polyphenol was informed. Thus, the formation of protein-polyphenol complexes can significantly reduce emulsion droplet size or help maintain a small and stable particle size distribution under thermal and salt stress (Li et al. 2021).

3.4 | Antioxidant Capacity After Digestion

Previous reports (Rubinstein and Pérez 2025) had demonstrated an additive effect on antioxidant capacity upon complex formation evaluated at pH 9 by QP-RSV and QP-TOC. However, to consider these complexes as potential functional ingredients, it is necessary to evaluate their behavior upon gastrointestinal digestion. This was assessed using three complementary techniques.

The ABTS assay was performed as the initial step. A limitation encountered here was the high inherent antiradical capacity of the digestive enzymes by their own. The samples that

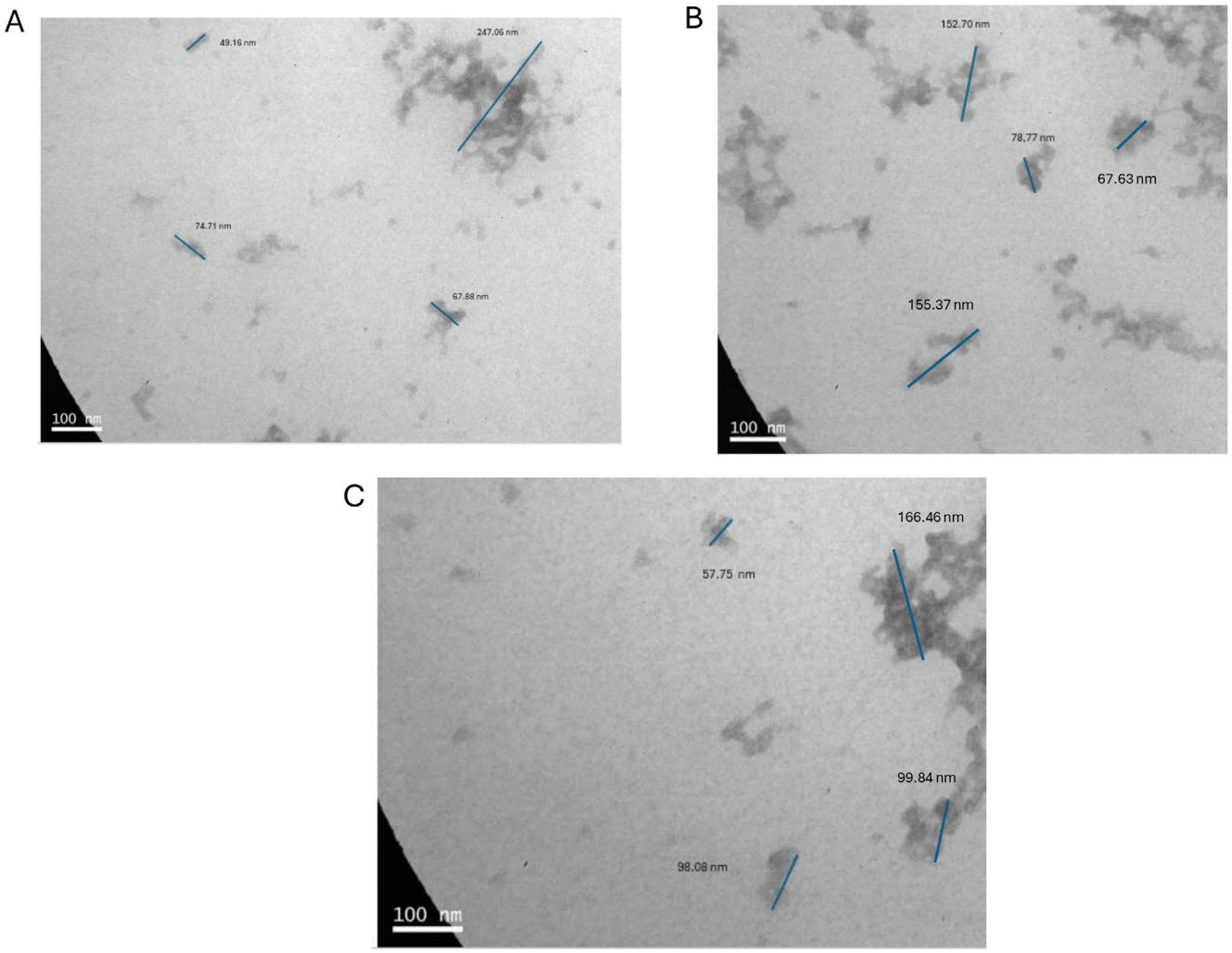

FIGURE 1 | TEM images of QP (A), QP-RSV (B), and QP-TOC (C).

went through in vitro digestion could not be measured directly by this method and were diluted at a 1:5 ratio. (Figure 2A). Furthermore, a strong increase in antiradical capacity was observed in all samples upon digestion.

Figure 2B presents the results obtained from the FRAP assay, before and after in vitro digestion. As observed, in all cases, the antioxidant capacity increases after each stage of the digestion process. This was a positive outcome, as it indicates that the antioxidant potential was not only preserved but also enhanced throughout digestion, allowing it to reach the intestinal tract. The analysis of the protein-bioactive mixtures reveals that, prior to in vitro digestion, their total antioxidant capacity demonstrated an additive effect, being approximately the sum of the individual components. This had already been reported in previous studies for a QP concentrate (Rubinstein and Pérez 2025).

The final antioxidant capacity of the digested complexes was increased compared to their predigestion state. Furthermore, the primary objective of creating these protein-bioactive nanocomplexes was often to protect the labile bioactive compound during food processing and shelf-life, ensuring its stability and delivery, which is a key advantage beyond the scope of this specific post-digestion antioxidant assay.

The final analysis involved determining antioxidant capacity through the hydrogen peroxide method. Here, much like with the ABTS assay, the blank's antioxidant capacity, stemming from the digestive enzymes themselves, was found to be very high. Crucially, a consistent increase in antioxidant activity after in vitro digestion was observed across all samples.

The data presented across the three assays (ABTS, FRAP, and Hydrogen Peroxide) consistently demonstrate that the antioxidant capacity of all tested compounds (RSV, TOC, QP) and their combinations resulted significantly enhanced when analyzed upon simulated in vitro digestion assay. This outcome, including the activity of the blank, is largely expected and aligns with previous findings in the literature (Wu et al. 2022). The results shown here are consistent with findings from other studies. For example, Wu et al. (2022) found the antioxidant activity of curcumin-myofibrillar protein complexes, measured by both DPPH and ABTS radical scavenging rates, significantly

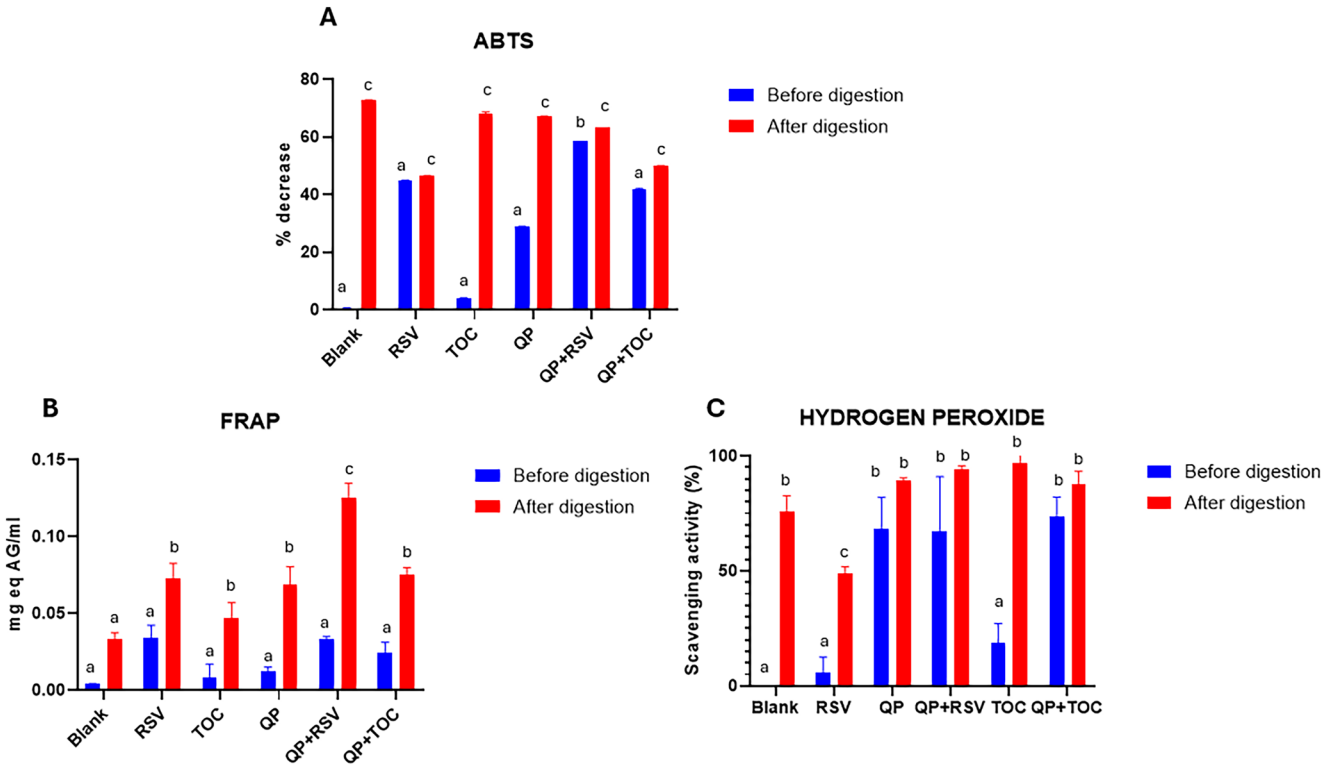

FIGURE 2 | Antioxidant capacity evaluated by ABTS (A), FRAP (B), and Hydrogen peroxide (C) in TOC or RSV mixed systems prior to and after in vitro digestion. Results are expressed as mean ± SD, $n = 3$ ($p < 0.05$).

decreased in the initial stages of the in vitro digestion. However, with extended digestion time, the scavenging rates of the curcumin-MP complexes increased, which was attributed to the release of more antioxidant-capable polypeptides due to the presence of curcumin. Also, de Morais et al. (2020) found that in the control samples, isolated phenolic compounds degraded under simulated gastrointestinal conditions. In contrast, complexation with whey protein isolate (WPI) protected the phenolic compounds from degradation, enhancing their stability. While WPI alone showed weak antioxidant capacity, its digestibility was improved, releasing small peptides with antioxidant activity. The variation in performance across the different assays was expected, as each method probes a distinct antioxidant mechanism.

4 | Conclusions

In this study, nanocomplexes formed by QP and either RSV or TOC were formed and characterized. The understanding of these complexes was enhanced through the analysis by various analytical methodologies, including FTIR and TEM microscopy. The EE of both compounds was measured and falls within the range of other bioactive compounds and encapsulation platforms, that is, nanocomplexes. Additionally, the nanocomplexes and their individual components were subjected to an in vitro digestion process. The antioxidant capacity of the digested compounds was evaluated, revealing an increase in this property whatever the methodology used. These results indicate that the complexes could be strong candidates for their use as functional food ingredients.

Author Contributions

Alejandra J. Rubinstein: conceptualization, formal analysis, investigation, validation, visualization, writing – original draft. **Guadalupe Garcia Liñares:** resources, supervision, writing – review and editing. **Valeria Boeris:** resources, supervision, writing – review and editing. **Oscar E. Pérez:** conceptualization, funding acquisition, project administration, resources, supervision, writing – review and editing. All authors have read and agreed to the published version of the manuscript.

Acknowledgments

This work was supported by the Universidad de Buenos Aires—UBA (UBACYT N° 20020190100297BA); the Agencia Nacional de Promoción Científica y Tecnológica—ANPCyT (PICT 2021-0347); and the Consejo Nacional de Investigaciones Científicas y Técnicas—CONICET (PIP 2022-2024 GI 11220210100072CO).

Funding

This work was supported by the Secretaría de Ciencia y Técnica, Universidad de Buenos Aires (20020190100297BA), the Consejo Nacional de Investigaciones Científicas y Técnicas (PIP 2022-2024 GI 11220210100072CO), and the Agencia Nacional de Promoción Científica y Tecnológica (PICT 2021-0347).

Ethics Statement

The authors have nothing to report.

Conflicts of Interest

The authors declare no conflicts of interest.

References

Akhtar, N., N. Akhtar, F. Menaa, et al. 2022. "Fabrication of Ethosomes Containing Tocopherol Acetate to Enhance Transdermal Permeation: In Vitro and Ex Vivo Characterizations." *Gels* 8, no. 6: 335. https://doi.org/10.3390/gels8060335.

Andreeva, Y. I., A. S. Drozdov, A. F. Fakhardo, N. A. Cheplagin, A. A. Shtil, and V. V. Vinogradov. 2017. "The Controllable Destabilization Route for Synthesis of Low Cytotoxic Magnetic Nanospheres With Photonic Response." *Scientific Reports* 7, no. 1: 11343. https://doi.org/10.1038/s41598-017-11673-4.

Buosi, F. S., A. Alaimo, M. C. Di Santo, et al. 2020. "Resveratrol Encapsulation in High Molecular Weight Chitosan-Based Nanogels for Applications in Ocular Treatments: Impact on Human ARPE-19 Culture Cells." *International Journal of Biological Macromolecules* 165: 804–821. https://doi.org/10.1016/j.ijbiomac.2020.09.234.

Bustos, L. F., F. E. Vasile, and O. E. Pérez. 2024. "Experimental and in Silico Approaches for the Buffalo Whey Protein-Folic Acid Complexation Elucidation. Molecular Changes Impacting on Protein Structure and Functionality." *Food Research International* 180: 114062. https://doi.org/10.1016/j.foodres.2024.114062.

Chimento, A., F. De Amicis, R. Sirianni, et al. 2019. "Progress to Improve Oral Bioavailability and Beneficial Effects of Resveratrol." *International Journal of Molecular Sciences* 20, no. 6: 1381. https://doi.org/10.3390/ijms20061381.

De Matteo, R., J. M. Rey, R. Corfield, et al. 2024. "Chitosan-Inspired Matrices for Folic Acid. Insightful Structural Characterization and Ensured Bioaccessibility." *Food Biophysics* 19: 412–424. https://doi.org/10.1007/s11483-024-09833-x.

de Morais, F. P. R., T. B. Pessato, E. Rodrigues, L. Peixoto Mallmann, L. R. B. Mariutti, and F. M. Netto. 2020. "Whey Protein and Phenolic Compound Complexation: Effects on Antioxidant Capacity Before and After in Vitro Digestion." *Food Research International* 133: 109104. https://doi.org/10.1016/j.foodres.2020.109104.

Demirkaya, F., and Y. Kadioglu. 2007. "Simple GC-FID Method Development and Validation for Determination of α-Tocopherol (Vitamin E) in Human Plasma." *Journal of Biochemical and Biophysical Methods* 70, no. 3: 363–368. https://doi.org/10.1016/j.jbbm.2006.08.006.

Haris, P. I., and D. Chapman. 1995. "The Conformational Analysis of Peptides Using Fourier Transform IR Spectroscopy." *Biopolymers* 37, no. 4: 251–263. https://doi.org/10.1002/bip.360370404.

He, X., B. Wang, B. Zhao, and F. Yang. 2022. "Ultrasonic Assisted Extraction of Quinoa (*Chenopodium quinoa* Willd.) Protein and Effect of Heat Treatment on Its in Vitro Digestion Characteristics." *Food* 11, no. 5: 771. https://doi.org/10.3390/foods11050771.

Li, M., C. Ritzoulis, Q. Du, et al. 2021. "Recent Progress on Protein-Polyphenol Complexes: Effect on Stability and Nutrients Delivery of Oil-in-Water Emulsion System." *Frontiers in Nutrition* 8: 1–16. https://doi.org/10.3389/fnut.2021.765589.

Lingiardi, N., M. Galante, M. de Sanctis, and D. Spelzini. 2022. "Are Quinoa Proteins a Promising Alternative To Be Applied in Plant-Based Emulsion Gel Formulation?" *Food Chemistry* 394: 133485. https://doi.org/10.1016/j.foodchem.2022.133485.

Martínez, J. H., F. Velázquez, H. P. Burrieza, et al. 2019. "Betanin Loaded Nanocarriers Based on Quinoa Seed 11S Globulin. Impact on the Protein Structure and Antioxidant Activity." *Food Hydrocolloids* 87: 880–890. https://doi.org/10.1016/j.foodhyd.2018.09.016.

Pérez, O. E., T. David-Birman, E. Kesselman, S. Levi-Tal, and U. Lesmes. 2014. "Milk Protein-Vitamin Interactions: Formation of Beta-Lactoglobulin/Folic Acid Nano-Complexes and Their Impactoninvitro Gastro-Duodenal Proteolysis." *Food Hydrocolloids* 38: 40–47. https://doi.org/10.1016/j.foodhyd.2013.11.010.

Pleh, A., L. Mahmutović, and A. Hromić-Jahjefendić. 2021. "Evaluation of Phytochemical Antioxidant Levels by Hydrogen Peroxide Scavenging Assay." *Bioengineering Studies* 2, no. 1: 1–10. https://doi.org/10.37868/bes.v2i1.id178.

Roxana Bancuta, O., A. Chilian, I. Bancuta, R. Setnescu, T. Setnescu, and R. Mariana Ion. 2018. "Thermal Characterization of Resveratrol." http://www.revistadechimie.ro.

Rubinstein, A. J., G. G. Liñares, V. Boeris, and O. E. Pérez. 2024. "An Innovative Bio-Vehicle for Resveratrol and Tocopherol Based on Quinoa 11S Globulin-Nanocomplex Design and Characterization." *Pharmaceutics* 16: 1118. https://doi.org/10.3390/pharmaceutics16091118.

Rubinstein, A. J., and O. E. Pérez. 2025. "Quinoa Proteins Isolate, a Candidate for Functional Ingredients Design." *Plant Foods for Human Nutrition* 80, no. 1: 7. https://doi.org/10.1007/s11130-024-01242-2.

Saini, R. K., and Y. S. Keum. 2016. "Tocopherols and Tocotrienols in Plants and Their Products: A Review on Methods of Extraction, Chromatographic Separation, and Detection." *Food Research International* 82: 59–70. https://doi.org/10.1016/j.foodres.2016.01.025.

Schwaighofer, A., M. R. Alcaráz, C. Araman, H. Goicoechea, and B. Lendl. 2016. "External Cavity-Quantum Cascade Laser Infrared Spectroscopy for Secondary Structure Analysis of Proteins at Low Concentrations." *Scientific Reports* 6: 33556. https://doi.org/10.1038/srep33556.

Shahidi, F., and A. C. De Camargo. 2016. "Tocopherols and Tocotrienols in Common and Emerging Dietary Sources: Occurrence, Applications, and Health Benefits." *International Journal of Molecular Sciences* 17, no. 10: 1–29. https://doi.org/10.3390/ijms17101745.

Skvarnavičius, G., Z. Toleikis, V. Michailovienė, C. Roumestand, D. Matulis, and V. Petrauskas. 2021. "Protein-Ligand Binding Volume Determined From a Single 2D NMR Spectrum With Increasing Pressure." *Journal of Physical Chemistry B* 125, no. 22: 5823–5831. https://doi.org/10.1021/acs.jpcb.1c02917.

Wu, C., H. Dong, P. Wang, M. Han, and X. Xu. 2022. "Sequential Changes in Antioxidant Activity and Structure of Curcumin-Myofibrillar Protein Nanocomplex During in Vitro Digestion." *Food Chemistry* 382: 132331. https://doi.org/10.1016/j.foodchem.2022.132331.

Supporting Information

Additional supporting information can be found online in the Supporting Information section. **Figure S1:** FTIR spectra of TOC, QP, and QP + TOC (A), RSV, QP and QP + RSV (B). **Figure S2:** Curve-fitted second derivative of amide I region (1700–1600 cm^{-1}) of QP (A), QP + RSV (B), QP + TOC (C) and secondary structure elements of the samples (D).